A finite difference formulation inspired by the pseudopotential lattice Boltzmann method

Luiz Eduardo Czelusniak[a,c], luiz.czelusniak@partner.kit.edu,

Alfredo Jaramillo Palma[b], alfredo.jaramillo@uwyo.edu,

Luben Cabezas-Gómez[a,*] , lubencg@sc.usp.br, (55)(16) 3373-9531, (55)(16) 98217-2353

[a]Heat Transfer Research Group, Department of Mechanical Engineering, São Carlos School of Engineering, University of São Paulo, Trabalhador São-carlense Avenue, 400, 13566-590, São Carlos, SP, Brazil.

[b]Center of Innovation for Flow Through Porous Media, University of Wyoming, 651 N 19th St, Laramie, WY, 82072, United States.

[c]Lattice Boltzmann Research Group, Department of Mathematics, Karlsruhe Institute of Technology, Building 20.30, Englerstraße 2, 76131, Karlsruhe, Baden-Württemberg, Germany.

[*]Author for correspondence

Authors short bibliographical description:

Luiz Eduardo Czelusniak obtained his PhD in Mechanical Engineering from the São Carlos School of Engineering at the University of São Paulo, São Paulo, Brazil. He completed post-doctorate studies at the Center for Energy and Petroleum Studies at the State University of Campinas, Campinas, Brazil. He is currently a postdoctoral fellow at the Karlstuhe Institute of Technology in Germany. Works in the area of numerical simulation of thermal and fluidic systems with the lattice Boltzmann method.

Alfredo Jaramillo Palma acts as Senior Research Scientist in the Center of Innovation for Flow through Porous Media, University of Wyoming, Fort Collins, Colorado, US. He focuses in the following main topics: the numerical simulation of flows in porous media, of gas-liquid phase change problems with the lattice Boltzmann method and on hydrodynamic lubrication simulation.

Luben Cabezas Gómez acts as Associate Professor in the Mechanical Engineering Department at São Carlos School of Engineering, University of São Paulo, São Paulo, Brazil. He focuses on the following main topics: the numerical simulation of thermal systems and heat exchangers and the numerical simulation of gas–liquid flows with phase change in heat exchangers with the lattice Boltzmann method and computational fluid dynamics techniques.

A finite difference formulation inspired by the pseudopotential lattice Boltzmann method

Abstract: The pseudopotential method has grown as a powerful tool for multiphase fluid flow simulations in the lattice Boltzmann method framework. We consider that due to its simplicity and computational efficiency, the pseudopotential method could also be explored in the framework of more traditional Computational Fluid Dynamic methods such as Finite Difference, Finite Volume, or Finite Element methods. Following this idea, in this work, we discretize the macroscopic equations resulting from the pseudopotential lattice Boltzmann method by a simple Finite Difference scheme. This finite difference method is then studied in different benchmark problems such as a planar interface, a smooth droplet oscillation, and a single droplet evaporation. Excellent results were obtained in all tests. One of the advantages of the proposed Finite Difference method is that mesh refinement can be done straightforwardly, and converged solutions can be used as a tool to validate the lattice Boltzmann method. The results indicate that the pseudopotential method is suitable to be used with standard discretization methods such as Finite Difference and that in future works more robust discretizations can be used to further enhance the pseudopotential method application.

Keywords: Lattice Boltzmann method, Pseudopotential method, Finite Difference Method, Multiphase fluid flows, Macroscopic balance equations.

1. Introduction

The application of the pseudopotential lattice Boltzmann method (LBM) [1, 2, 3] for multiphase fluid flow simulation has gained much attention in the scientific community. This method does not require the interface to be tracked or captured since different phases are maintained in coexistence due to the action of a fluid-fluid interaction force. The interaction force acting at a specific node depends on the density and temperature of the neighbor nodes. The pseudopotential method has been applied in the simulation of single bubble nucleation [4], pool boiling [4, 5, 6, 7], flow boiling in microchannels [8], flow boiling in a vertical channel under conjugate heat transfer [9], impact and droplet boiling on heated surfaces [10], and to study the effect of wettability and structured surfaces in pool boiling heat transfer efficiency [11, 12, 13, 14, 15, 16].

Many works of the pseudopotential literature focus on qualitative results, whereas only a few works consider quantitative aspects such as mesh refinement (showing that the solution is grid independent), or analysis of numerical artifacts like spurious currents. The reason why it is uncommon to see mesh refinement analyses with the pseudopotential method is because this procedure is far from trivial, involving modifications to the parameters of the equation of state, and precomputations that involve steady-state simulations, as shown by Jaramillo et al. [17]. In this last work, it was also shown the necessity of obtaining numerically converged solutions for modeling correctly the desired physical process, e.g., the pool boiling phenomenon. Recently, to obtain a comparative solution for the LBM simulations, the present authors developed a simple Finite Difference (FD) method to solve the macroscopic conservation equations resulting from the pseudopotential method for simple problems, which could also be easily refined [18]. This raised the question of whether the pseudopotential method could be successfully used for multiphase simulations by employing standard discretization methods such as Finite Difference or Finite Volume methods.

The topic of FD formulations inspired by LBM was explored by several authors in the literature. Fučík and Straka et al. [19] developed a general procedure based on recursive substitutions to obtain equivalent FD methods from LBM for Navier-Stokes equations (NSE). Belloti et al. [20] demonstrated that any lattice Boltzmann scheme can be rewritten as a corresponding multi-step FD scheme on the conserved variables, considering mainly

the NSE. Equivalent macroscopic FD schemes of LB methods for the one-dimensional diffusion and convection-diffusion equations were obtained by [21, 22] and [23], respectively. Recently Liu et al. [24] developed a macroscopic FD scheme to solve NSE and convection-diffusion equations, considering the evolution of hydrodynamic variables of NSE itself, requiring much less memory resources.

When FD is applied to multiphase simulation, the technique is usually combined with a front tracking method [25]. However, FD methods are rarely applied to multiphase simulations compared to other methods such as volume of fluid (usually based on Finite Volume) [25]. In the present paper, a macroscopic FD formulation from the pseudopotential LBM is proposed to simulate multiphase flow.

The good features of the pseudopotential method could make it suitable for simulations using standard discretization methods. More robust discretizations could enhance some features of the method such as its stability for phase-change simulations under low reduced temperatures, which is a great challenge nowadays in the LBM literature [26]. In this work, we test the applicability of the pseudopotential method with standard discretization schemes for different multiphase and phase-change simulations involving heat transfer. For this, a simple FD scheme based on central isotropic stencils in space and a second-order explicit Runge-Kutta in time is chosen. The benchmark tests are the planar interface, the smooth droplet oscillation, and the evaporation of a single droplet.

2. Theoretical Background

2.1. Pseudopotential Method

The pseudopotential method has its origin in the interaction force proposed by Shan and Chen [1]. This interaction force acting on the fluid was able to maintain different fluid phases in coexistence allowing the simulation of multiphase flow. From another point of view, we can consider that by adding the interaction force F_α^{int} into the momentum conservation equation we are changing the original pressure tensor $P_{\alpha\beta}^{old}$ of the system to a new non-ideal pressure by writing $-\partial_\beta p_{\alpha\beta}^{new} = \partial_\beta p_{\alpha\beta}^{old} + F_\beta^{\text{int}}$ (α and β denote vector and tensor components, and the summation convention of Einstein is adopted). Typically, the natural pressure tensor given by the isothermal lattice Boltzmann method is

$\partial_\beta p_{\alpha\beta}^{old} = \rho c_s^2 \delta_{\alpha\beta}$ where c_s is the lattice sound speed and ρ is the fluid density. In general, when the interaction force is applied in the pseudopotential method this pressure tensor assumes the new form:

$$p_{\alpha\beta}^{new} = \left(\rho c_s^2 + \frac{Gc^2}{2}\psi^2 + A\frac{Gc^4}{12}\left(\partial_\gamma \psi\right)\left(\partial_\gamma \psi\right) + (B-C)\frac{Gc^4}{12}\psi\partial_\gamma\partial_\gamma\psi \right)\delta_{\alpha\beta} + C\frac{Gc^4}{12}\psi\partial_\alpha\partial_\beta\psi \,, \quad (1)$$

where ψ is called "effective density" or "interaction potential" in the literature [27, 28]. The coefficients A, B and C influence different multiphase properties of the method such as interface thickness and surface tension [29] (α, β and γ denote tensor components). In two dimensions, these indices assume values in $\{x, y\}$. In three dimensions, they assume values in $\{x, y, z\}$. The summation convention of Einstein is adopted.

Originally, Shan and Chen [1] adopted $\psi = \rho_0\left[1-\exp\left(\rho/\rho_0\right)\right]$, and the parameter G was used to control the interaction strength. Also, c is a parameter that depends on the magnitude of the lattice velocities adopted in the lattice Boltzmann method [27]. Most authors adopt a configuration where $c = 1$.

According to Eq. (1), in the absence of gradients of the effective density ψ, the pressure tensor simplifies to $p_{\alpha\beta} = p\delta_{\alpha\beta}$, with $p = \rho c_s^2 + Gc^2\psi^2/2$. This expression motivated Yuan and Schaefer [30] to use the effective density ψ to add a new equation of state P_{EOS} to the system:

$$\psi\left(\rho, T\right) = \sqrt{\frac{2\left(P_{EOS}(\rho, T) - \rho c_s^2\right)}{Gc^2}}\,, \quad (2)$$

where T is the temperature of the fluid. When this technique is used, G no longer controls the interaction strength. Replacing Eq. (2) into Eq. (1), one can see that the dependency on G is eliminated. Instead, G can be seen as an auxiliary parameter to keep positive the term inside the square root. Typically, the parameters of the EOS are set in such a way that $P_{EOS} < \rho c_s^2$. In that case, the value $G = -1$ can be adopted.

2.2. Phase Densities at Mechanical Equilibrium

For a system modeled by an equation of state P_{EOS}, when two phases are in thermodynamic equilibrium separated by a planar interface, the Maxwell equal area rule states that the densities of the fluid corresponding to each phase must satisfy the condition:

$$\int_{v_l}^{v_v} \left(p_0 - P_{EOS} \right) dv = \int_{\rho_v}^{\rho_l} \left(p_0 - P_{EOS} \right) \frac{d\rho}{\rho^2}, \tag{3}$$

where ρ_v and ρ_l are the vapor- and liquid-saturated densities, and p_0 is the bulk pressure. Considering a fluid modeled by Eq. (1) with two phases in equilibrium separated by a planar interface, and imposing $\partial_\alpha p_{\alpha\beta} = 0$, the following expression for the pseudopotential vapor-liquid relation can be derived [31]:

$$\int_{\rho_v}^{\rho_l} \left(p_0 - \rho c_s^2 - \frac{G c_s^2}{2} \psi^2 \right) \frac{\dot{\psi}}{\psi^{1+\varepsilon}} d\rho = \int_{\rho_v}^{\rho_l} \left(p_0 - P_{EOS} \right) \frac{\dot{\psi}}{\psi^{1+\varepsilon}} d\rho, \tag{4}$$

where $\varepsilon = -2A/B$, A and B are the pressure tensor coefficients of Eq. (1). By adjusting the parameter ε we can make Eq. (4) be satisfied for the same densities given by the Maxwell rule in Eq. (3). Note that the equilibrium densities for a flat interface do not depend on coefficient C. Following the analysis conducted in Czelusniak et al. [29] it is observed that coefficient C can be adjusted to control the method surface tension.

3. Finite Difference Method

In this section, the partial differential equations that are implied by the pseudopotential method are presented. These macroscopic conservative equations are discretized using simple finite difference schemes with central stencils for the space derivatives and a second-order Runge-Kutta method for the time discretization.

3.1. Macroscopic Governing Equations

The mass, momentum, and energy conservation equations obtained from the pseudopotential method can be written as:

$$\partial_t \rho + \partial_\gamma \left(\rho u_\gamma \right) = 0, \tag{5a}$$

$$\partial_t \left(\rho u_\alpha \right) + \partial_\beta \left(\rho u_\alpha u_\beta \right) = -\partial_\beta P_{\alpha\beta} + F_\alpha + \partial_\beta \sigma'_{\alpha\beta}, \tag{5b}$$

$$\partial_t T = -u_\gamma \partial_\gamma T + \frac{1}{\rho c_v}\partial_\gamma\left(\kappa \partial_\gamma T\right) - \frac{T}{\rho c_v}\left(\frac{\partial P_{EOS}}{\partial T}\right)\partial_\gamma u_\gamma , \tag{5c}$$

in Eq. (5b) the viscous stress tensor $\sigma'_{\alpha\beta}$ reads:

$$\sigma'_{\alpha\beta} = \mu\left(\partial_\alpha u_\beta + \partial_\beta u_\alpha\right) + \mu_B \delta_{\alpha\beta}\partial_\gamma u_\gamma , \tag{6}$$

with μ being the shear viscosity and μ_B a coefficient of viscosity used to control the bulk viscosity. Usually, authors define the bulk viscosity as the combination $\left(2/3\mu + \mu_B\right)$ [27]. The effects of the pseudopotential fluid-fluid interaction that causes the phase separation were incorporated inside the pressure tensor which has the same form of Eq. (1). In this work, we are fixing the coefficients $B = 3$ and $C = 2$ for simplicity. In this case, only coefficient $A = -\varepsilon B/2$ can be varied to control the equilibrium phase densities (see Eq. (4)). The values of A used in this work will be provided in the following sections since they depend on the equation of state and fluid temperature. The effective density ψ used in this work follows the definition given in Eq. (2).

3.2. FD Discretization

In this work, the space derivatives are discretized using the same type of central stencils used to discretize the interaction forces in the lattice Boltzmann method following Czelusniak et al. [29]:

$$M^1_\alpha\left(\varphi(x)\right) \triangleq \sum_k w_k c_{k\alpha}\varphi\left(x + c_k\Delta x\right) = \left(\Delta x\right)c_s^2\partial_\alpha\varphi\left(x\right) + O\left(\Delta x^3\right), \tag{7a}$$

$$M^2_{\alpha\beta}\left(\varphi(x)\right) \triangleq \sum_k w_k\left(c_{k\alpha}c_{k\beta} - c_s^2\delta_{\alpha\beta}\right)\varphi\left(x + c_k\Delta x\right) = (\Delta x)^2 c_s^4\partial_\alpha\partial_\beta\varphi\left(x\right) + O\left(\Delta x^4\right). \tag{7b}$$

Here, the values of w_k and c_k are set such that Eqs. (7a) and (7b) are satisfied, i.e., such that $M^1_\alpha\left(\varphi(x)\right)/\Delta x$ and $M^2_\alpha\left(\varphi(x)\right)/(\Delta x)^2$ are second order approximations of $c_s^2\partial_\alpha\varphi\left(x\right)$ and $c_s^4\partial_\alpha\partial_\beta\varphi\left(x\right)$, respectively. In this work w_k are given by $w_0 = 4/9$, $w_{1,2,3,4} = 1/12$ and $w_{5,6,7,8} = 1/36$. The values of c_k are $c_0 = (0,0)$, $c_{1,3} = \left(\pm 1, 0\right)$, $c_{2,4} = \left(0, \pm 1\right)$, and $c_{5,6,7,8} = \left(\pm 1, \pm 1\right)$. Finally, $c_s^2 = 1/3$.

From Eq. (7a), one has that:

$$\partial_\gamma\left(\rho u_\gamma\right)\approx\frac{M_\gamma^1\left(\rho u_\gamma\right)}{\left(\Delta x\right)c_s^2},\ \partial_\beta\left(\rho u_\alpha u_\beta\right)\approx\frac{M_\beta^1\left(\rho u_\alpha u_\beta\right)}{\left(\Delta x\right)c_s^2},$$
$$\partial_\gamma\left(T\right)\approx\frac{M_\gamma^1\left(T\right)}{\left(\Delta x\right)c_s^2},\qquad\partial_\gamma\left(\rho u_\gamma\right)\approx\frac{M_\gamma^1\left(u_\gamma\right)}{\left(\Delta x\right)c_s^2}. \tag{8}$$

To discretize the divergence of the viscous stress tensor $\partial_\beta\sigma'_{\alpha\beta}$, it is first observed that:

$$\begin{aligned}\partial_\beta\sigma'_\beta=&\left(\partial_\beta\mu\right)\left(\partial_\alpha u_\beta+\partial_\beta u_\alpha\right)+\mu\left(\partial_\alpha\partial_\beta u_\beta+\partial_\beta\partial_\beta u_\alpha\right)\\&+\left(\partial_\alpha\mu_B\right)\partial_\gamma u_\gamma+\mu_B\partial_\alpha\partial_\beta u_\beta.\end{aligned} \tag{9}$$

Since the dynamic viscosities μ and μ_B can also be functions of ρ, the $\partial_\beta\mu$ and $\partial_\alpha\mu_\beta$ can be expressed as:

$$\partial_\beta\mu=\left(\partial_\rho\mu\right)\left(\partial_\alpha\rho\right),\quad\partial_\alpha\mu_B=\left(\partial_\rho\mu_B\right)\left(\partial_\alpha\rho\right). \tag{10}$$

Thus, to discretize the term $\partial_\beta\sigma'_{\alpha\beta}$, one can replace Eq. (10) into Eq. (9) and then discretize all spatial derivatives using Eqs. (7a) and (7b). The discretization of the term $\partial_\gamma\left(\kappa\partial_\gamma T\right)$ in the energy equation follows a similar path. Writing $\partial_\gamma\left(\kappa\partial_\gamma T\right)=\left(\partial_\gamma\kappa\right)\left(\partial_\gamma T\right)+\kappa\partial_\gamma\partial_\gamma T$ and applying Eqs. (7a) and (7b).

The discretization of the pressure tensor divergence $\partial_\beta p_{\alpha\beta}$ is done in two steps: First, the pressure tensor (1) is computed with the spatial derivatives of the effective density being approximated by:

$$\partial_\gamma\varphi\approx\frac{M_\gamma^1\left(\varphi\right)}{\left(\Delta x\right)c_s^2},\ \partial_\gamma\partial_\gamma\varphi\approx\frac{M_{\gamma\gamma}^2\left(\varphi\right)}{\left(\Delta x\right)^2c_s^4},\ \partial_\alpha\partial_\beta\varphi\approx\frac{M_{\alpha\beta}^2\left(\varphi\right)}{\left(\Delta x\right)^2c_s^4}. \tag{11}$$

Then, the pressure tensor divergence can be approximated as:

$$\partial_\beta p_{\alpha\beta}\approx\frac{M_\beta^1\left(p_{\alpha\beta}\right)}{\left(\Delta x\right)c_s^2}. \tag{12}$$

The term F_α in Eq. (5b) represents the action of an external force field on the fluid. One example of such an external force field is gravity. Such forces are disregarded in this work.

Assuming a computational domain ranging from $x_0\le x_i\le x_f$, $y_0\le y_i\le y_f$ and time ranging from $t_0\le t_n\le t_f$, we discretize the domain using an amount of nodes: N_x for x-

direction, N_y for y-direction and N_t for time. We can write $x_i = x_0 + i\Delta x$, $y_i = y_0 + j\Delta y$ and $t_n = t_0 + n\Delta t$, where $0 \le i \le N_x - 1$, $0 \le j \le N_y - 1$, $0 \le n \le N_t - 1$ and $\Delta x = \left(x_f - x_0\right)/\left(N_x - 1\right)$, $\Delta y = \left(y_f - y_0\right)/\left(N_y - 1\right)$ and $\Delta t = \left(t_f - t_0\right)/\left(N_t - 1\right)$. Now variables like $\rho(t, x, y)$ can be represented by indexes as ${\rho_{i,j}}^n$. Using Eqs. (5a), (5b) and (5c) and the space discretizations described in this section we can write the derivatives as functions of the time and space coordinate such as: $\partial_t {\rho^n}_{i,j} = f_\rho\left(t_n, x_i, y_i\right)$, $\partial_t \left(\rho u_x\right)^n_{i,j} = f_{\rho u_x}\left(t_n, x_i, y_i\right)$, $\partial_t \left(\rho u_y\right)^n_{i,j} = f_{\rho u_y}\left(t_n, x_i, y_i\right)$, and $\partial_t T^n_{i,j} = f_T\left(t_n, x_i, y_i\right)$. Then, we use second-order explicit Runge-Kutta time-discretization scheme. Its first step reads:

$$\rho^{n+1/2}_{i,j} = \rho^n_{i,j} + \frac{\Delta t}{2} f_\rho\left(t_n, x_i, y_i\right),\ T^{n+1/2}_{i,j} = T^n_{i,j} + \frac{\Delta t}{2} f_T\left(t_n, x_i, y_i\right), \tag{13a}$$

$$\left(\rho u_x\right)^{n+1/2}_{i,j} = \left(\rho u_x\right)^n_{i,j} + \frac{\Delta t}{2} f_{\rho u_x}\left(t_n, x_i, y_i\right),\ \left(\rho u_y\right)^{n+1/2}_{i,j} = \left(\rho u_y\right)^n_{i,j} + \frac{\Delta t}{2} f_{\rho u_y}\left(t_n, x_i, y_i\right), \tag{13b}$$

where $n+1/2$ denotes time-evaluation at $t_n + \Delta t/2$. After computing the variables for all grid nodes, the second step is performed:

$$\rho^{n+1}_{i,j} = \rho^n_{i,j} + \Delta t\ f_\rho\left(t_{n+1/2}, x_i, y_i\right),\ T^{n+1}_{i,j} = T^n_{i,j} + \Delta t\ f_{\rho u_y}\left(t_{n+1/2}, x_i, y_i\right), \tag{14a}$$

$$\begin{aligned} \left(\rho u_x\right)^{n+1}_{i,j} &= \left(\rho u_x\right)^n_{i,j} + \Delta t\ f_{\rho u_x}\left(t_{n+1/2}, x_i, y_i\right), \\ \left(\rho u_y\right)^{n+1}_{i,j} &= \left(\rho u_y\right)^n_{i,j} + \Delta t\ f_{\rho u_y}\left(t_{n+1/2}, x_i, y_i\right), \end{aligned} \tag{14b}$$

Notice that the pseudopotential method is based on the fact that the LBM is a weak-compressible method. This means that the pressure field is not computed from the Poisson equation, but from the EOS and thus from its dependency on the density field, which, on its own, is computed from the mass conservation equation. There, the interaction force acts changing the density of the fluid continuously between the respective vapor and liquid values, the region where this transition between vapor and liquid takes place is identified as *interface*. Thus, at every time step, the EOS pressure and the function ψ - Eq. (2) - must be updated with the new density values. If the viscosity is density-dependent, it also must be updated for every time step. Also, it is worth noticing that a key point of the pseudopotential method is that the Mach number should be maintained below 0.3 to

approach the limit of incompressibility. In this way, the simulation will approach a multiphase flow with incompressible bulk phases.

4. Numerical Results

The simulations in this section are carried out using two equations of state, namely the Carnahan-Starling (C-S) EOS [30, 32] and the Peng-Robinson (P-R) EOS. These equations are used in the same form as presented by Yuan and Schaefer [30]. The C-S EOS depends on three parameters (a, b, and R), here these values are set as $a = 0.5$, $b = 5$, and $R = 1$. Whereas the P-R EOS depends on four parameters (a, b, R, and ω), which were set as $a = 3/49$, $b = 2/21$, $R = 1$ and $\omega = 0.344$. These are values commonly used in LBM literature [30, 32].

The values of A in Eq. (1) are computed from Eq. (4). First, for a certain EOS, the equilibrium densities are computed for each temperature from Eq. (3). Then, these equilibrium densities are inserted in Eq. (4). These equations are then solved numerically to obtain ε, and by consequence A. The computed values of A are shown in Table (1) up to $T_r = 0.8$ for the C-S EOS. For higher temperatures, it is possible to use the same value computed for $T_r = 0.8$ with negligible error.

Table 1: Values of A coefficient for different EOS and temperatures.

LBM simulations are performed to compare the numerical results of two tests, the smooth droplet oscillation and the evaporation of a single droplet. For the pseudopotential LBM, we use the numerical scheme proposed by Li et al. [32] with the same parameters used in the finite difference simulations. This kind of simulation is usually performed in a unit system called 'lattice units', where the grid spacing is taken as $\Delta x = 1$, and the time step is taken as $\Delta t = 1$. In this way, the number of nodes $\left(N_x, N_y\right)$ are equal to the domain size $\left(L_x, L_y\right)$. As a reference, we adopt our coarsest grid in the finite difference method with $\Delta x = 1$, maintaining the same spatial resolution as in the LBM simulation. The time step in the FD simulations is set as $\Delta t = 0.8(\Delta x)^2$. Such a time step ensured numerical

stability during the mesh refinement procedure. All simulations were done employing an in-house code implemented in C and Matlab^{R}.

4.1. Planar Interface

The planar interface problem is schematized in Fig. 1. The goal here is to evaluate if the coexistence densities match the ones given by the Maxwell equal area rule when two phases separated by a planar interface reach equilibrium. The physical domain has a rectangular geometry with sides $\left(L_x, L_y\right) = \left(200, 2\right)$. The density field is initialized as a diffuse planar interface given by the function:

$$\rho\left(x, y\right) = \frac{\rho_v + \rho_l}{2} + \frac{\rho_l - \rho_v}{2}\left(\tanh\left[4.6\frac{\left(x - x_1\right)}{W} \right] - \tanh\left[4.6\frac{\left(x - x_2\right)}{W} \right] \right), \qquad (15)$$

Where $x_1 = 0.25L_x$ and $x_2 = 0.75L_x$ are the locations of the interfaces, and W is the interface width, set to $W = 10$. The fluid is modeled by the C-S EOS. For a specific temperature, the values of ρ_v and ρ_l are initialized as the saturated densities obtained by applying the Maxwell rule to the C-S EOS. The kinematic viscosity coefficients are set as $\nu = \mu / \rho = 0.06$ and $\nu_B = \mu_B / \rho = 0$. The velocity field is initialized with null components and at all boundaries periodic boundary conditions are applied. The simulations are conducted until $t = 20000$ to allow the system to reach the steady state. The computation of ε is necessary to make the pseudopotential method coexistence densities equal to the ones given by the Maxwell rule. The value of ε for each temperature is obtained by numerically solving Eq. (4) following the procedure described in [26]. Three different grid spacing values were utilized $\Delta x = 1$, $\Delta x = 1/2$, and $\Delta x = 1/4$.

Figure 1: One-dimensional configuration for the planar interface problem. The spatial dependency takes place only along the coordinate x. Liquid and vapor regions are separated by an interface, and periodic conditions are set at the left and right sides.

Figure 2: (a) Coexistence curve for C-S EOS with different Δx values. (b) Relative error for the vapor densities at different reduced temperatures.

The coexistence curves, obtained numerically, are shown in Fig. (2.a), and compared against the curve predicted by the Maxwell rule. Good agreement between the numerical curve and the Maxwell rule is observed for the liquid density in all the ranges T_r. For the vapor densities, good agreement is observed for most of the range of T_r. However, some deviation is observed at lower temperature values when the density ratio becomes large. These deviations are quantified in Fig. (2.b), where the relative error is computed as $100\left(\rho_v - \rho_v^M\right)/\rho_v^M$, with ρ_v denoting the value obtained numerically, and ρ_v^M denoting the value given by the Maxwell rule. As mentioned, for low reduced temperatures the relative error for the vapor phase density grows, reaching a value as high as 50% for $\Delta x = 1$. This can be explained by the fact that errors increase when the density ratio also increases. The density ratio grows exponentially when the temperature is reduced. These large errors at high-density ratios also occur for the lattice Boltzmann method [18].

It can also be observed that the relative error reduces when the mesh is refined. In Fig. (2.b), the result for $T_r = 0.5$ is not shown for $\Delta x = 1/4$ since the simulation was turned out unstable in that case. This issue may be related with the particular choice of the FD scheme, which is not the focus of this work. Thus, other choices may be tested in future research.

The results shown in Fig. (2.b) indicate that the method is consistent and approaches the Maxwell rule when Δx is reduced. Also, is observed that the vapor densities are accurate at $T_r \geq 0.7$, even for the coarsest mesh.

Figure 3: Relative error of the vapor density for different grid scales. Numerical results are relative to FD simulations. The other lines show the tendency of the error.

Fig. (3) shows the error behavior for different mesh sizes at $T_r = 0.6$. The grid spacing is gradually reduced down to $\Delta x = 1/8$. In that Figure, the numerical results relative to the FD simulations are also shown, together with reference lines. It is observed that the error of the method tends to zero quadratically.

4.2. Smooth Droplet Oscillation

For this test, a liquid droplet is initialized with an elliptic profile in such a way that its shape oscillates smoothly in a vapor medium. The physical domain has a square geometry of $\left(L_x, L_y\right) = (100,100)$. The initial shape of the droplet (with a diffuse interface) is initialized using the formulae [29]

$$\rho(x,y) = \frac{\rho_v + \rho_l}{2} - \frac{\rho_l - \rho_v}{2}\left(\tanh\left[2\frac{(R - R_0)}{W}\right]\right),\ R_0(\theta) = \frac{R_{\min}}{\sqrt{1-\left[e\cos\theta\right]^2}}, \tag{16a}$$

$$\theta(x,y) = \arctan\left(\frac{y-y_0}{x-x_0}\right),\ \ e = \sqrt{1-\left(\frac{R_{\min}}{R_{\max}}\right)^2}, \tag{16b}$$

Where $R = \sqrt{(x-x_0)^2 + (y-y_0)^2}$, $W = 5$, $R_{\max} = 35$, and $R_{\min} = 25$. The C-S EOS is used with $T_r = 0.6$. The vapor and liquid densities ρ_v and ρ_l at this temperature are obtained by applying the Maxwell equal area rule. Periodic boundary conditions are imposed.

This kind of simulation requires setting the viscosity to a small value to avoid the dissipation of the oscillations. It was observed that $\nu = 0.033$ and $\nu_B = 0$ were appropriate values, but simulations became unstable with the mesh refinement. Following an idea from the LBM literature [32] to increase stability we set different viscosities for the vapor and liquid region by defining the density-dependent kinematic viscosities ν and ν_B:

$$\nu = \nu_l\left(\frac{\rho-\rho_v}{\rho_l-\rho_v}\right) + \nu_v\left(\frac{\rho_l-\rho}{\rho_l-\rho_v}\right),\ \ \nu_B = \nu_{B,v}\left(\frac{\rho-\rho_v}{\rho_l-\rho_v}\right) + \nu_{B,l}\left(\frac{\rho_l-\rho}{\rho_l-\rho_v}\right). \tag{17}$$

it was found that the values $\nu_l = 0.033$, $\nu_v = 0.1$, $\nu_{B,l} = 0.067$ and $\nu_{B,v} = 0$ allowed stable simulation for all meshes. The evolution of the droplet in time is shown in Fig. (4). In Fig. (4.b) it is shown that simulations with all mesh sizes provided close values of amplitude and oscillation frequency.

Figure 4: Droplet radius along time for the elliptic droplet oscillation. (a) Snapshots of FD simulation ($\Delta x = 1$) at different times (in lattice units). (b) Comparison between FD (with different meshes) and LBM (with $\Delta x = 1$). The average radius is defined as $R_m = \sqrt{R_{\min} R_{\max}}$.

A comparison between the LBM simulation with the FD simulation is shown in Fig. (4.b). Both methods provided close results, although the LBM simulation needs to be refined to fit better the FD refined simulation results. As explained by [17], the LBM mesh refinement procedure for two-phase flows is cumbersome, involving modifications to the parameters of the equation of state. Due to the small differences observed in Fig. (4.b), this procedure is not applied in this case.

Simulation times for the LBM and FD simulation with the coarse mesh were logged. Both codes were implemented in C. The LBM simulation took 33 seconds, and the FD simulation took 268 seconds in an Intel(R) Core(TM) i7-4510U CPU @ 2.00GHz 2.00 GHz processor using 4 cores. As a first work about this topic, we are using a very simple discretization strategy. However, as a drawback, this strategy is not as computationally efficient as LBM. In future works, different strategies may be tested to improve the efficiency of the FD scheme.

4.3. Droplet Evaporation

In this last test, FD is compared with the LBM in a phase change problem. This is done by simulating the evaporation process of a liquid droplet surrounded by warmed vapor inside an enclosed cavity, which corresponds to a widely employed benchmark problem in the LBM literature [33, 34]. The FD scheme used to solve the energy conservation equation is similar to the one applied by Li et al. [35] with central isotropic schemes for the spatial derivatives. However, a second-order explicit Runge-Kutta scheme was utilized instead of the fourth-order scheme applied by the authors. The lattice configuration is the same as used in the previous tests with $\left(L_x, L_y\right) = \left(100,100\right)$. A circular liquid droplet of radius $R_0 = 20$ is initialized in the center of the domain using Eq. (16a) and considering null velocities. Notice that now R_0 is constant and not a function of θ since it is a circular

droplet. The saturation densities are computed at the saturation temperature of $T_{sat} = 0.86T_c$, utilizing the Maxwell equal area rule. For this simulation, the P-R EOS was employed as this equation is widely utilized in the LBM literature for phase change problems. Following [34] and [29], the temperature of the liquid droplet is set as being equal to the saturation temperature $T_{sat} = 0.86T_c$, whereas the vapor region is set to the higher temperature $T_v = T_{sat} + \Delta T$ (with $\Delta T = 0.14T_c$), and for that the temperature profile is initialized using the same function used for the density profile. In this way, the temperature on the interface of the droplet changes smoothly. The rest of the physical parameters are thermal conductivity $\lambda = 2/3$, specific heat capacity $c_v = 5$, and kinematic viscosity coefficients $\nu = 0.1$, and $\nu_B = 0$. The interface width is set to $W = 5$. Two different meshes were employed for the calculations of the FD method: $\Delta x = 1$, and $\Delta x = 1/2$.

Figure 5: (a) Snapshots for evaporating droplets at different instants of time. (b) Comparison of the droplet diameter along time for the FD simulations with two mesh sizes and the LBM for $\Delta x = 1$.

Snapshots for the density profile at different moments are shown in Fig. (5.a) for the FD method using $\Delta x = 1/2$. This test was also simulated using the hybrid pseudopotential model proposed by [35]. Both the FD method and the LBM provided close results, as observed in Fig. (5.b), where the diameter of the droplet, $D(t)$, is shown over time. At the beginning of the simulation, the droplet shrinks faster than during the rest of the simulation, probably due to the large gap in temperature between the liquid and vapor regions. After some time, $D(t)$ followed the well-known D^2 law [36, 37], where $D(t)^2$ decreases linearly with t.

5. Conclusions and future work

The proposed FD scheme for the pseudopotential macroscopic conservation equations produced correct results for the three test problems. These three problems are numerically challenging, indicating that the proposed simulation procedure is useful, and can be employed for evaluating other numerical methods. The procedure allows us to perform grid

refinement studies to investigate the dependency of the solution with the mesh in a classical form, i.e., considering only the mesh size decrease without the modification of other parameters, as it is commonly required for the LBM. This is a very useful characteristic inherited from the FD method. In future works, envisioning the utilization of the pseudopotential method in phase-change problems at low reduced temperatures, more robust time discretization schemes (such as semi-implicit schemes) could be used to enhance stability and to allow the usage of a wider range of viscosities.

6. Acknowledgements

The authors acknowledge the support received from CNPq (National Council for Scientific and Technological Development, process 305941/2020-8) and FAPESP (São Paulo Foundation for Research Support, 2016/09509-1, 2018/09041-5, and 2020/12919-2), for developing research that has contributed to this study. The authors also fully acknowledge the insights and contributions of Prof. Alexander Wagner from North Dakota State University (NDSU) to the present paper.

References

[1] Shan, X. and Chen, H. “Lattice boltzmann model for simulating flows with multiple phases and components”, *Physical Review E*, 47(3), pp. 1815-1820 (1993). DOI: 10.1103/PhysRevE.47.1815

[2] Shan, X. and Chen, H. “Simulation of nonideal gases and liquid-gas phase transitions by the lattice boltzmann equation”, *Physical Review E*, 49(4), pp. 2941-2948 (1994). DOI: 10.1103/PhysRevE.49.2941

[3] Pattnaik, A.C., Samanta, R., and Chattopadhyay, H. “A brief on the application of multiphase lattice boltzmann method for boiling and evaporation”, *Journal of Thermal Analysis and Calorimetry*, 148, pp. 2869-2904 (2023). DOI: 10.1007/s10973-022-11820-8

[4] Guzella, M.S., Czelusniak, L.E., Mapelli, V.P., et al. “Simulation of boiling heat transfer at different reduced temperatures with an improved pseudopotential lattice boltzmann method”, *Symmetry*, 12(8), pp. 1358 (2020). DOI: 10.3390/sym12081358

[5] Ma, X. and Cheng. P. “3D simulations of pool boiling above smooth horizontal heated surfaces by a phase-change lattice boltzmann method”, *International Journal of Heat and Mass Transfer*, 131, pp. 1095–1108 (2019). DOI: 10.1016/j.ijheatmasstransfer.2018.11.103

[6] Gong, S. and Cheng. P. “Direct numerical simulations of pool boiling curves including heater’s thermal responses and the effect of vapor phase’s thermal conductivity”, *International Communications in Heat and Mass Transfer*, 87, pp. 61–71 (2017). DOI: 10.1016/1.icheatmasstransfer.2017.06.023

[7] Zhao, W., Liang, J., Sun, M., et al. “Investigation on the effect of convective outflow boundary condition on the bubbles growth, rising and breakup dynamics of nucleate boiling”, *International Journal of Thermal Sciences*, 167, pp. 106877 (2021). DOI: 10.1016/j.ijthermalsci.2021.106877

[8] Zhang, C., Chen, L., Ji, W., et al. “Lattice boltzmann mesoscopic modeling of flow boiling heat transfer processes in a microchannel”, *Applied Thermal Engineering*, 197, pp; 117369 (2021). DOI: 10.1016/j.applthermaleng.2021.117369

[9] Guo, Y., Lai, Y., Wang, S., et al. “Modelling of bubble dynamics on vertical rough wall with conjugate heat transfer”, *Applied Thermal Engineering*, 234, pp. 121268 (2023). DOI: 10.1016/j.applthermaleng.2023.121268

[10] Xu, Y., Tian, L., Zhu, C., et al. “Impact and boiling characteristics of a droplet on heated surfaces: a 3d lattice boltzmann study”, *Applied Thermal Engineering*, 219, pp. 19360 (2023). DOI: 10.1016/japplthermaleng.2022.119360

[11] Li, Q., Yu, Y., Zhou, P., et al. “Enhancement of boiling heat transfer using hydrophilic-hydrophobic mixed surfaces: a lattice boltzmann study”, *Applied Thermal Engineering*, 132, pp. 490–499 (2018). DOI: 10.1016/j.applthermaleng.2017.12.105

[12] Li, W.X., Li, Q., Yu, Y., et al. “Nucleate boiling enhancement by structured surfaces with distributed wettability-modified regions: a lattice boltzmann study”, *Applied Thermal Engineering*, 194, pp; 117130 (2021). DOI: 10.1016/j.applthermaleng.2021.117130

[13] Feng, Y., Chang, F., Hu, Z., et al. “Investigation of pool boiling heat transfer on hydrophilic-hydrophobic mixed surface with micro-pillars using LBM”, *International Journal of Thermal Sciences*, 163, pp. 106814 (2021). DOI: 10.1016/j.ijthermalsci.2020;106814

[14] Fedoseev, A.V., Salnikov, M.V., Ostapchenko, A.E., et al. “Lattice boltzmann simulation of optimal biphilic surface configuration to enhance boiling heat transfer”, *Energies*, 15(21), pp. 8204 (2022). DOI: 10.3390/en15218204

[15] Wang, J., Liang, G., Yin, X., et al. “Pool boiling on micro-structured surface with lattice boltzmann method”, *International Journal of Thermal Sciences*, 187, pp. 108170 (2023). DOI: 10.1016/j.ijthermalsci.2023.108170

[16] Ezzatneshan, E., Salehi, A., and Vaseghnia, H. “Study of micro-heater shape and wettability effects on inception of boiling phenomenon using a multiphase lattice boltzmann method”, *International Journal of Thermal Sciences*, 184, pp. 107913 (2023). DOI: 10.1016/j.ijthermalsci.2022.107913

[17] Jaramillo, A., Mapelli, V.P., and Cabezas-Gómez, L. “Pseudopotential lattice boltzmann method for boiling heat transfer: A mesh refinement procedure”, *Applied Thermal Engineering*, 213, pp, 118705 (2022). DOI: 10.1016.j.applthermaleng.2022.118705

[18] Czelusniak, L.E. *Estudo da aplicação do método de Boltzmann em rede do pseudopotencial em simulações bifásicas gás-líquido*, PhD thesis, Universidade de São Paulo, (2022).

[19] Fučík, R. and Straka, R. “Equivalent finite difference and partial differential equations for the lattice boltzmann method”, *Computers & Mathematics with Applications*, 90, pp. 96–103 (2021). DOI: 10.1016.j.camwa.2021.03.014

[20] Bellotti, T., Graille, B., and Massot, M. “Finite difference formulation of any lattice boltzmann scheme”, *Numerische Mathematik*, 152(1), pp. 1–40 (2022). DOI: 10.1007/s00211-022-01302-2

[21] Lin, Y., Hong, N., Shi, B., et al. “Multiple-relaxation-time lattice boltzmann model-based four-level finite-difference scheme for one-dimensional diffusion equations”, *Physical Review E*, 104(1), pp. 015312 (2021). DOI: 10.1103/PhysRevE.104.015312

[22] Silva, G. “Discrete effects on the source term for the lattice boltzmann modelling of one-dimensional reaction–diffusion equations”, *Computers & Fluids*, 251, pp. 105735 (2023). DOI: 10.1016/j.compfluid.2022.105735

[23] Chen, Y., Chai, Z., and Shi, B. “Fourth-order multiple-relaxation-time lattice boltzmann model and equivalent finite-difference scheme for one-dimensional convection-

diffusion equations", *Physical Review E*, 107(5), pp. 055305 (2023). DOI: 10.1103/PhysRevE.107.055305

[24] Liu, X., Chen, Y., Chai, Z., et al. "Macroscopic finite-difference scheme based on the mesoscopic regularized lattice-boltzmann method", *Physical Review E*, 109(2), pp. 025301 (2024). DOI: 10.1103/PhysRevE.109.025301

[25] Tiwari, A., Samanta, R., and Chattopadhyay, H. "Droplet solidification: physics and modelling", *Applied Thermal Engineering*, 228, pp. 120515 (2023). DOI: 10.1016/applthermaleng.2023.120515

[26] Czelusniak, L.E., Mapelli, V.P., Wagner, A.J., et al. "Shaping the equation of state to improve numerical accuracy and stability of the pseudopotential lattice boltzmann method", *Physical Review E*, 105, pp. 015303 (2022). DOI: 10.1103/PhysRevE.105.015303

[27] Krüger, T., Kusumaatmaja, H., Kuzmin, A., et al. *The lattice boltzmann method. principles and practice*, Springer International Publishing, 1st Ed., pp. 694 (2017). DOI: 10.1007/978-3-319-44649-3

[28] Mapelli, V.M., Czelusniak, L.E., Guzella, M.S., et al. "On the force scheme influence on pseudopotential method coexistence curve", *Physica A: Statistical Mechanics and its Applications*, 599, pp. 127411 (2022). DOI: 10.1016.j.physa.2022.127411

[29] Czelusniak, L.E., Mapelli, V.P., Guzella, M.S., et al. "Force approach for the pseudopotential lattice boltzmann method", *Physical Review E*, 102(3), pp. 033307 (2020). DOI: 10.1103/PhysRevE.102.033307

[30] Yuan P. and Schaefer, L. "Equations of state in a lattice boltzmann model", *Physics of Fluids*, 18(4), pp. 042101 (2006). DOI: 10.1063/1.2187070

[31] Shan, X. "Pressure tensor calculation in a class of nonideal gas lattice boltzmann models", *Physical Review E*, 77(6), pp. 066702 (2008). DOI: 10.1103/PhysRevE.77.066702

[32] Li, Q., Luo, K.H., and Li, X.J. "Lattice boltzmann modeling of multiphase flows at large density ratio with an improved pseudopotential model", *Physical Review E*, 87(5), pp. 053301 (2013). DOI: 10.1103/PhysRevE.87.053301

[33] Li, Q., Kang, Q.J., François, M.M., et al. "Lattice boltzmann modeling of self-propelled leidenfrost droplets on ratchet surfaces", *Soft Matter*, 12(1), pp. 302–312 (2016). DOI: 10.1039/C5SM01353D

[34] Li, Q., Zhou, P., and Yan, H.J. "Improved thermal lattice boltzmann model for simulation of liquid-vapor phase change", *Physical Review E*, 96(6), pp. 063303 (2017). DOI: 10.1103/PhysRevE.96.063303

[35] Li, Q., Kang, Q.J., François, M.M., et al. "Lattice boltzmann modeling of boiling heat transfer: The boiling curve and the effects of wettability", *International Journal of Heat and Mass Transfer*, 85, pp. 787–796 (2015). DOI: 10.1016/j.ijheatmasstransfer.2015.01.136

[36] Safari, H., Rahimian, M.H., and Krafczyk, M. "Extended lattice boltzmann method for numerical simulation of thermal phase change in two-phase fluid flow", *Physical Review E*, 88(1), pp. 013304 (2013). DOI: 10.1103/PhysRevE.88.013304

[37] Law, C.K. "Recent advances in droplet vaporization and combustion", *Progress in energy and combustion science*, 8(3), pp. 171–201 (1982). DOI: 10.1016.0360-1285(82)90011-9

List of Tables

List of Figures

- Figure 4: Droplet radius along time for the elliptic droplet oscillation. (a) Snapshots of FD simulation ($\Delta x=1$) at different times (in lattice units). (b) Comparison between FD (with different meshes) and LBM (with $\Delta x=1$). The average radius is defined as $R_m = \sqrt{R_{\min} R_{\max}}$.

- Figure 5: (a) Snapshots for evaporating droplets at different instants of time. (b) Comparison of the droplet diameter along time for the FD simulations with two mesh sizes and the LBM for $\Delta x=1$.

Table 1: Values of A coefficient for different EOS and temperatures.

T_r	0.5	0.55	0.6	0.65	0.7	0.75	0.8	0.86
A(C-S)	-2.8463	-2.8309	-2.8155	-2.8002	-2.7850	-2.7698	-2.7547	-
A(P-R)	-	-	-	-	-	-	-	2.4758

Figure 1

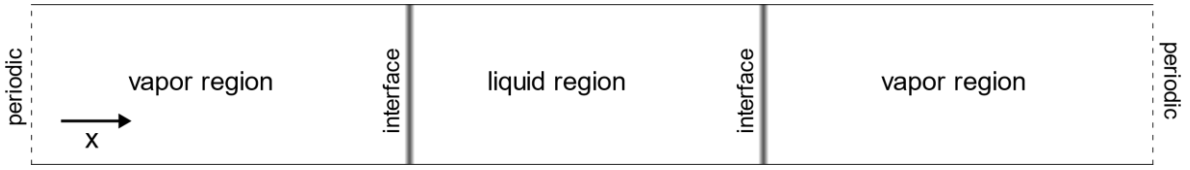

Figure 1: One-dimensional configuration for the planar interface problem. The spatial dependency takes place only along the coordinate x. Liquid and vapor regions are separated by an interface, and periodic conditions are set at the left and right sides.

Figure 2

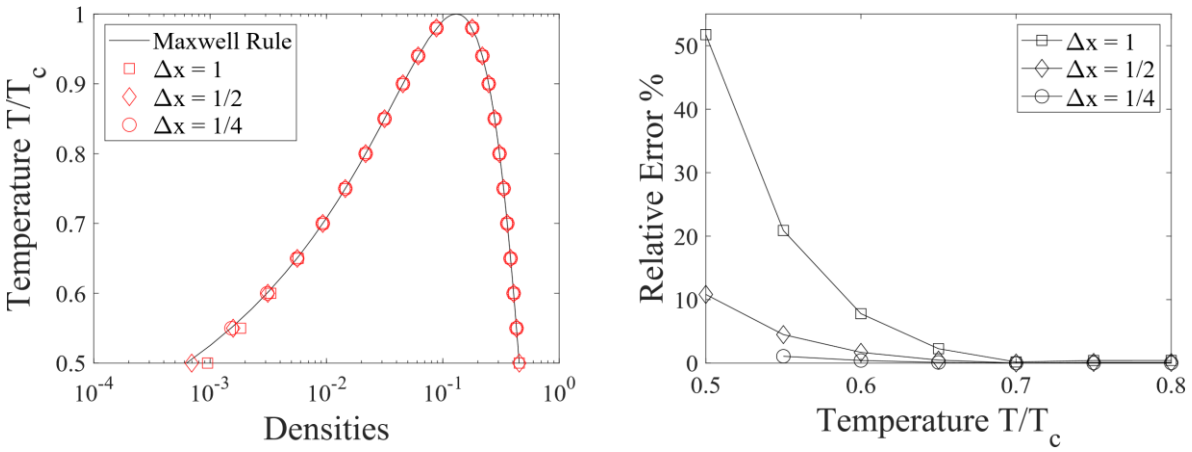

Figure 2: (a) Coexistence curve for C-S EOS with different Δx values. (b) Relative error for the vapor densities at different reduced temperatures.

Figure 3

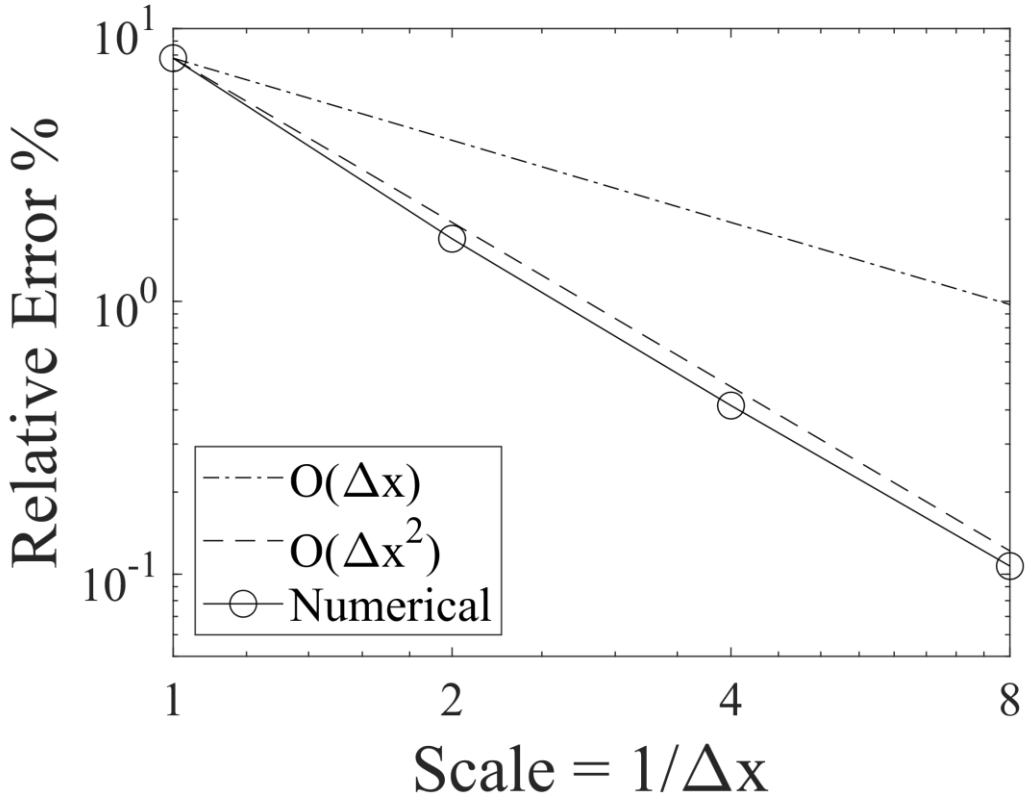

Figure 3: Relative error of the vapor density for different grid scales. Numerical results are relative to FD simulations. The other lines show the tendency of the error.

Figure 4

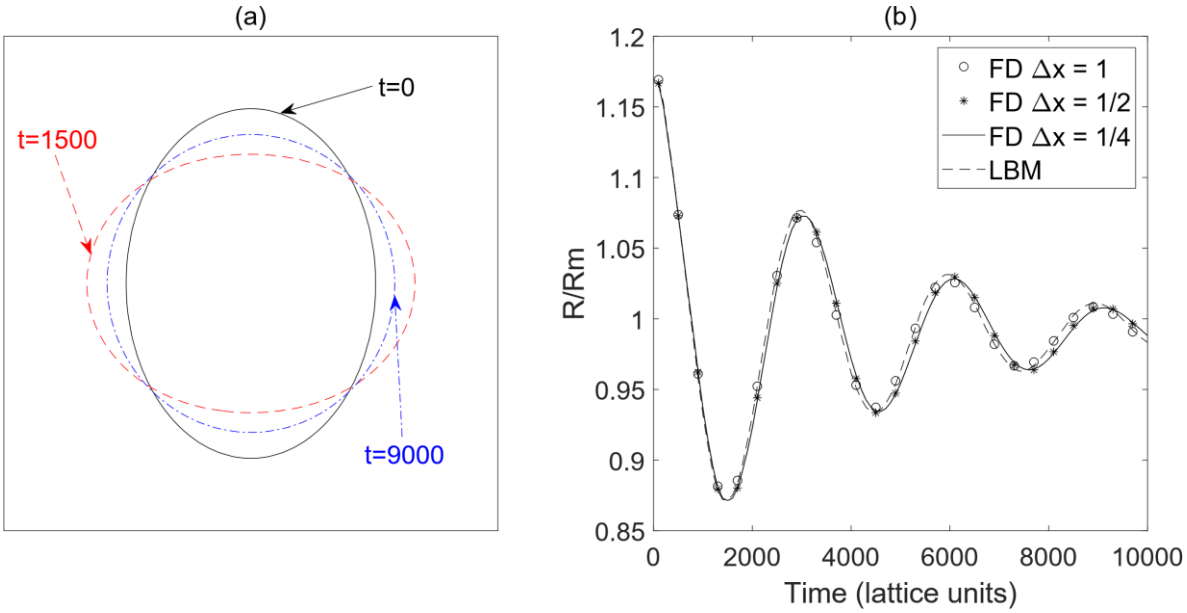

Figure 4: Droplet radius along time for the elliptic droplet oscillation. (a) Snapshots of FD simulation (Δx=1) at different times (in lattice units). (b) Comparison between FD (with different meshes) and LBM (with Δx=1). The average radius is defined as $R_m = \sqrt{R_{\min} R_{\max}}$.

Figure 5

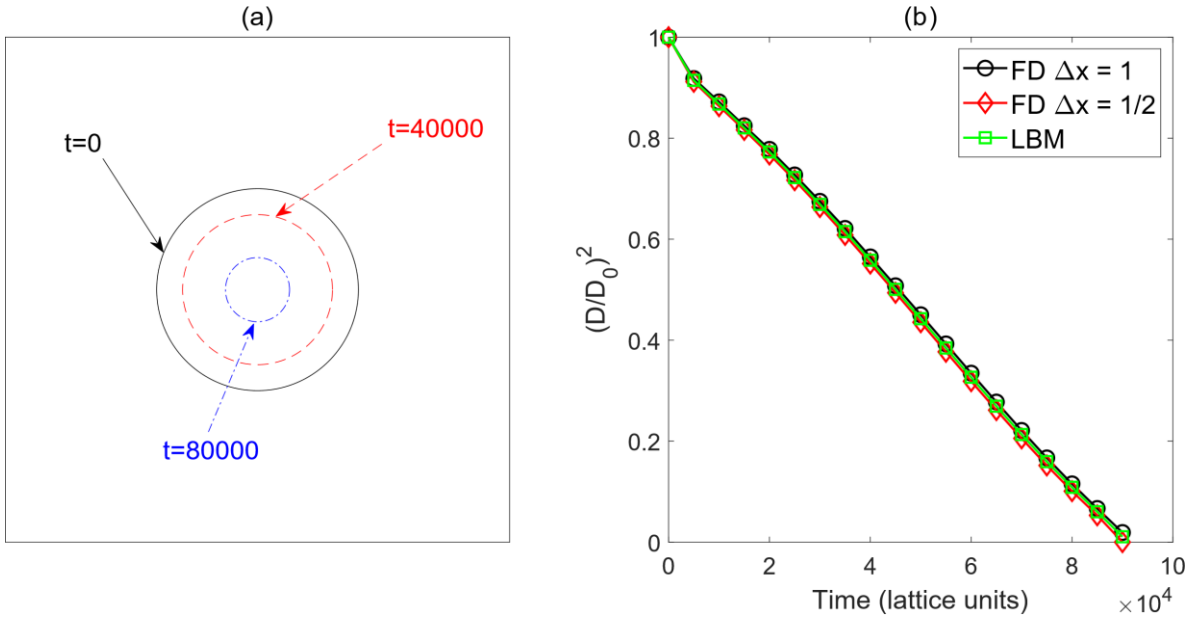

Figure 5: (a) Snapshots for evaporating droplets at different instants of time. (b) Comparison of the droplet diameter along time for the FD simulations with two mesh sizes and the LBM for $\Delta x=1$.